THE JOURNAL OF BIOLOGICAL CHEMISTRY VOL. 287, NO. 17, pp. 13829–13839, April 20, 2012

Complement-dependent Cytotoxicity in Neuromyelitis Optica Requires Aquaporin-4 Protein Assembly in Orthogonal Arrays*

Received for publication, January 18, 2012, and in revised form, February 26, 2012 Published, JBC Papers in Press, March 5, 2012, DOI 10.1074/jbc.M112.344325

Puay-Wah Phuan, Julien Ratelade, Andrea Rossi, Lukmanee Tradtrantip, and A. S. Verkman[1]

From the Departments of Medicine and Physiology, University of California, San Francisco, California 94143

Background: Complement-dependent cytotoxicity (CDC) plays a central role in neuromyelitis optica (NMO), in which NMO autoantibodies (NMO-IgG) bind to AQP4 on astrocytes.
Results: NMO-IgG produced CDC only when AQP4 was assembled in orthogonal arrays of particles (OAPs).
Conclusion: AQP4 assembly in OAPs is required for CDC by a mechanism involving multivalent C1q binding.
Significance: Our results establish a new mechanism of OAP-dependent pathogenesis in NMO and suggest a novel therapeutic strategy.

Neuromyelitis optica (NMO) is an inflammatory demyelinating disease of the central nervous system in which binding of pathogenic autoantibodies (NMO-IgG) to astrocyte aquaporin-4 (AQP4) causes complement-dependent cytotoxicity (CDC) and inflammation. We previously reported a wide range of binding affinities of NMO-IgGs to AQP4 in separate tetramers *versus* intramembrane aggregates (orthogonal arrays of particles, OAPs). We report here a second, independent mechanism by which CDC is affected by AQP4 assembly. Utilizing lactate dehydrogenase release and live/dead cell cytotoxicity assays, we found in different cell lines, and with different monoclonal and patient-derived NMO-IgGs, that CDC was greatly (>100-fold) reduced in cells expressing M1- *versus* M23-AQP4. Studies using a M23-AQP4 mutant containing an OAP-disrupting mutation, and in cells expressing AQP4 in different M1/M23 ratios, indicated that NMO-IgG-dependent CDC requires AQP4 OAP assembly. In contrast, antibody-dependent cell-mediated cytotoxicity produced by natural killer cells did not depend on AQP4 OAP assembly. Measurements of C1q binding and complement attack complex (C9neo) supported the conclusion that the greatly enhanced CDC by OAPs is due to efficient, multivalent binding of C1q to clustered NMO-IgG on OAPs. We conclude that AQP4 assembly in OAPs is required for CDC in NMO, establishing a new mechanism of OAP-dependent NMO pathogenesis. Disruption of AQP4 OAPs may greatly reduce NMO-IgG dependent CDC and NMO pathology.

Neuromyelitis optica (NMO)[2] is an inflammatory demyelinating disease of the central nervous system (CNS) with preponderance for lesions in spinal cord and optic nerve, leading to paralysis and blindness (1, 2). NMO lesions show prominent perivascular deposition of complement, as well as leukocyte infiltration and myelin loss (3, 4). A defining feature of NMO is the presence of autoantibodies (NMO-IgG) targeting aquaporin-4 (AQP4) (5, 6), a water channel expressed at the plasma membrane of astrocytes (7, 8). Evidence from cellular and rodent models suggests that NMO-IgG is pathogenic in NMO (9–12). NMO-IgG binding to AQP4 causes complement-dependent cytotoxicity (CDC), which initiates an inflammatory cascade involving cytokine release, leukocyte infiltration, microglial activation, and myelin loss (13, 14). Antibody-dependent cell-mediated cytotoxicity (ADCC) may also be involved. Current NMO therapies target the NMO-IgG load and inflammatory reaction (15, 16); also, the complement inhibitor Eculizumab is in an open label clinical trial. We recently introduced a monoclonal antibody ("aquaporumab") strategy to treat NMO in which a tight-binding, nonpathogenic anti-AQP4 antibody blocks NMO-IgG binding to AQP4 (17).

The target of the NMO autoantibody, AQP4, forms supramolecular assemblies in membranes called orthogonal arrays of particles (OAPs) (18, 19). We discovered the involvement of AQP4 in OAPs by showing OAPs in AQP4-transfected cells (20, 21) and the absence of OAPs in mice lacking AQP4 (22). We recently showed that NMO-IgG binding to AQP4 can be quite different when AQP4 is present in membranes as separate tetramers *versus* OAPs (23). Binding measurements were done using polyclonal NMO-IgG in NMO patient sera, as well as monoclonal recombinant NMO antibodies (NMO-rAb) derived from clonally expanded plasma blasts in cerebrospinal fluid of NMO patients. Although some antibodies bound similarly to AQP4 tetramers and OAPs, most antibodies bound with substantially higher affinity to AQP4 OAPs than tetramers. Mutagenesis studies and measurements of NMO-Fab binding suggested that OAP assembly causes a conformational change

* This work was supported, in whole or in part, by National Institutes of Health Grants EY13574, EB00415, DK35124, HL73856, DK86125, and DK72517 (to A. S. V.) This work was also supported by a grant from the Guthy-Jackson Charitable Foundation.

[1] To whom correspondence should be addressed: 1246 Health Sciences East Tower, University of California San Francisco, CA 94143-0521. Tel.: 415-476-8530; Fax: 415-665-3847; E-mail: Alan.Verkman@ucsf.edu.

[2] The abbreviations used are: NMO, neuromyelitis optica; AQP4, aquaporin-4; CDC, complement-dependent cytotoxicity; ADCC, antibody-dependent cell-mediated cytotoxicity; OAP, orthogonal arrays of particle; rAb, recombinant antibody; NK, natural killer; LDH, lactate dehydrogenase; TIRFM, total internal reflection fluorescence microscopy; BSS, balanced salt solution.

at the external AQP4 surface that influences NMO-IgG binding (23, 24).

Here, we investigated the role of OAP assembly by AQP4 in NMO-IgG-dependent cell killing by complement and natural killer cells, testing the hypothesis that efficient CDC requires OAP formation by AQP4 but that ADCC does not. The motivation for this study is the known multivalent interaction of complement protein C1q with antibody Fc region (25–27). We found greatly increased CDC for OAP-assembled AQP4, establishing a second mechanism by which NMO pathology is influenced by AQP4 assembly, independent of NMO-IgG binding.

EXPERIMENTAL PROCEDURES

DNA Constructs, Cell Lines, and Transfection—DNA constructs encoding full-length human AQP4 (M1 and M23 isoforms) and the M23 mutant G28P were generated and cloned into mammalian expression vector pcDNA3.1, as described (28). CHO-K1 cells (American Type Culture Collection (ATCC) CCL-61) were stably transfected with M1- and M23-AQP4 as described (21) and grown at 37 °C in 5% CO_2, 95% air in Ham's nutrient mix supplemented with 10% fetal calf serum, 100 units/ml penicillin, and 100 μg/ml streptomycin. U87MG cells (ATCC HTB-14) were stably transfected with M1- and M23-AQP4 as described (23) and cultured in Eagle's minimum essential medium containing 10% fetal bovine serum, 100 units/ml penicillin, and 100 μg/ml streptomycin. For transient transfections, U87MG cells were plated onto 96-well microplates (Costar, Corning Inc., Corning, NY) and transfected in antibiotic-free medium using Lipofectamine 2000 according to the manufacturer's instructions. Experiments were done 24 h after transfection. Human natural killer (NK) cells stably transfected with the Fc receptor CD16 (CD16-176V-NK92, Fox Chase Cancer Center, Philadelphia, PA) were cultured in α Minimum Essential Medium (Invitrogen) supplemented with 10% FBS, 10% horse serum, 2.5 mM L-glutamine, 100 μM β-mercaptoethanol, 1 mM sodium pyruvate, 2.5 μM folic acid, 0.2 mM *myo*-inositol, 100 units/ml penicillin, 100 μg/ml streptomycin, and 200 IU of human recombinant IL-2 (GenScript, Piscataway, NJ).

NMO Antibodies—NMO patient IgG (denoted NMO-IgG) was purified from serum of three NMO patients using a Melon gel IgG purification kit (Thermo Fisher Scientific) and concentrated using Amicon Ultra centrifugal filter units (Millipore, Billerica, MA). Recombinant monoclonal NMO antibodies (NMO-rAb; rAb-53; rAb-58) were generated from clonally expanded plasma blasts in cerebrospinal fluid of seropositive NMO patients as described (9). A non-NMO rAb (rAb-2B4) against measles virus nucleocapsid protein was used as a negative control antibody.

Binding Measurements—AQP4-expressing U87MG or CHO-K1 cells were incubated for 20 min in live cell blocking buffer (PBS containing 6 mM glucose, 1 mM sodium pyruvate, 1% bovine serum albumin, 2% goat serum) and then for 30 min with NMO-IgG or NMO-rAb in blocking buffer, as described (23). Cells were then rinsed in PBS, fixed in 4% paraformaldehyde for 15 min, and permeabilized with 0.1% Triton X-100. Cells were then blocked again and incubated for 30 min with 0.4 μg/ml polyclonal, C-terminal specific rabbit anti-AQP4 antibody (Santa Cruz Biotechnology, Santa Cruz, CA). Cells were then incubated for 30 min with 4 μg/ml goat anti-human IgG-conjugated Alexa Fluor 488 and goat anti-rabbit IgG-conjugated Alexa Fluor 555 (Invitrogen) in blocking buffer. Red and green fluorescence was imaged on a Nikon Eclipse TE2000S inverted epifluorescence microscope (Nikon, Melville, NY), and binding affinities were determined by nonlinear regression of background-subtracted green/red fluorescence intensity ratios.

Internalization Measurements—Cells cultured as described above were incubated with 50 μg/ml rAb-58 for 60 min at 23 and 37 °C. Cells were then washed extensively with cold PBS supplemented with 6 mM glucose and 1.1 mg/ml sodium pyruvate and blocked for 20 min in 1% BSA at 4 °C. As described (29), remaining AQP4 at the cell surface was labeled with 50 μg/ml rAb-58 at 4 °C for 1 h and then incubated with goat anti-human IgG-conjugated Alexa Fluor 555 (1:200, Invitrogen). The plasma membrane was stained using a fluorescent lectin, wheat germ agglutinin-conjugated Alexa Fluor 488 (1:400, Invitrogen). Cells were then washed and fixed for 15 min in 4% paraformaldehyde, and surface AQP4 was quantified as the (background-subtracted) ratio of red (surface AQP4) to green (plasma membrane) fluorescence. In some experiments, cells were exposed to 250 μg/ml NMO-IgGs purified from three different NMO sera for 60 min at 23 and 37 °C. Before labeling of surface AQP4 with rAb-58, bound purified IgGs at the cell surface were removed by acid wash in 0.2 M glycine, pH 2.5, for 15 s.

Total Internal Reflection Fluorescence Microscopy (TIRFM)—TIRFM was done on a Nikon Eclipse TE2000E microscope with a through-objective TIRF attachment and a 100× TIRF oil immersion objective (numerical aperture 1.49) mounted on a perfect focus module (Nikon), as described (23). Alexa Fluor 555-labeled AQP4 was excited using an argon ion laser through a Z514/10× excitation filter and imaged at 605 nm using a QuantEM 512SC deep-cooled CCD camera (Photometrics, Tucson, AZ).

CDC—CHO-K1 and U87MG cells were plated onto 96-well microplates (Costar, Corning) at 30,000 and 20,000 cells/well, respectively, and grown at 37 °C/5% CO_2 for 18–24 h. Cells were washed with Hanks' balanced salt solution (BSS) (without phenol red) and incubated at 23 or 37 °C for 60 min with NMO-IgG or NMO-rAb in Hanks' BSS containing 2% pooled normal human complement serum (Innovative Research, Novi, MI) in a final volume of 50 μl. To measure LDH release, the microplate was cooled to room temperature for 10 min, and 50 μl of CytoTox-ONE homogeneous membrane integrity assay solution (Promega, Madison, WI) was added according to the manufacturer's protocol. Complete (100%) LDH release was measured by the addition of 0.5 μl of 1% Triton X-100 to lyse cells. Background (0% lysis) LDH release was measured in cells incubated with complement but no NMO-IgG or NMO-rAb. LDH concentration was assayed from resorufin fluorescence measured on a TECAN Infinite M1000 plate reader (TECAN Groups Ltd., Mannedorf, Switzerland) (excitation/emission 560/590 nm). For live/dead cell staining, cells were washed with Hanks' BSS and then incubated with 1 μM calcein-AM (live cells, green fluorescence) and 2 μM ethidium homodimer-1 (dead cells, red fluorescence) (Invitrogen) in PBS for 15 min prior to imaging.

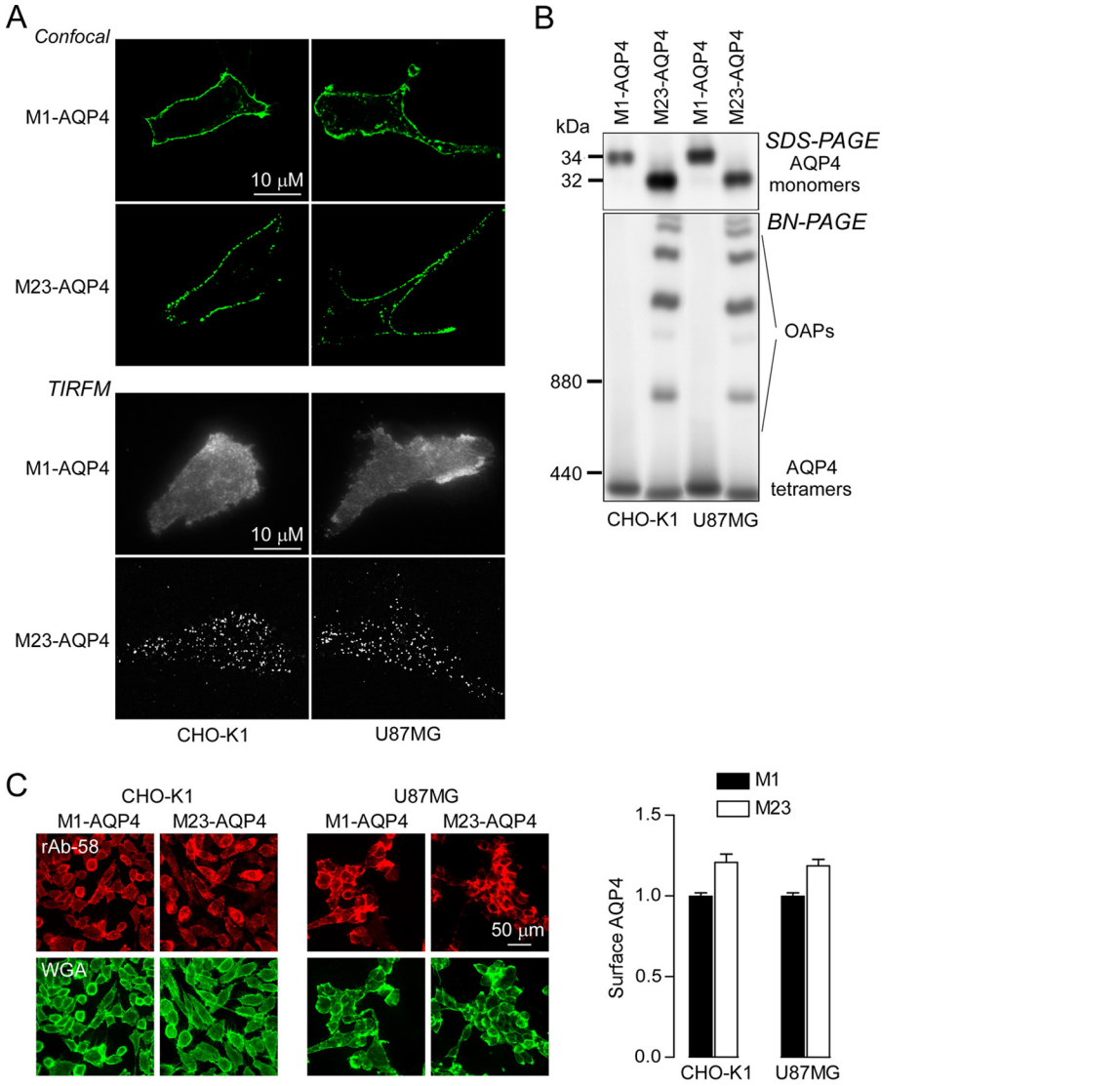

FIGURE 1. **Characterization of M1- and M23-AQP4-expressing CHO-K1 and U87MG cells.** *A*, confocal fluorescence microscopy (*top*) and TIRFM (*bottom*) of indicated cells immunostained for AQP4 using a C terminus anti-AQP4 antibody. *B*, SDS-PAGE (*top*) and Blue Native-PAGE (*BN-PAGE*, *bottom*) of cell homogenates. *C*, *left*, surface AQP4 expression quantified in live cells by immunostaining with 50 μg/ml rAb-58 for 1 h at 4 °C. Plasma membranes were stained with wheat germ agglutinin (*WGA*). *Right*, data are reported as the ratio of red (surface AQP4) to green (wheat germ agglutinin) fluorescence. (S.E., $n = 5$, *, $p < 0.01$).

ADCC—CHO-K1 cells were plated onto 96-well microplates (Costar, Corning) at 20,000 cells/well and grown at 37 °C/5% CO_2 for 18–24 h. Cells were then washed with PBS and incubated for 120 min at 37 °C with rAb-53 or rAb-58 (10 and 100 μg/ml), or control-rAb 2B4, and effector NK cells (effector: target ratio 30:1). Cells were washed gently with PBS to remove the remaining NK cells. 1 μM calcein-AM and 2 μM ethidium homodimer-1 were added for 30 min to stain live cells green and dead cells red.

C1q and C9neo Immunofluorescence—CHO-K1 cells were plated onto coverslips in 24-well plates and grown at 37 °C/5% CO_2 for 18–24 h. For C1q immunofluorescence, cells were washed with Hanks' BSS and incubated at room temperature for 30 min with 400 μl of Hanks' BSS containing 40 μg/ml rAb-58 and 120 μg/ml human C1q protein (Abcam, Cambridge, MA). Cells were washed with PBS, fixed in 4% paraformaldehyde for 15 min, and permeabilized with 0.1% Triton X-100. Cells were blocked with 1% BSA for 30 min and incubated for 60 min with 1:200 dilution of FITC-conjugated rabbit polyclonal anti-C1q antibody (Abcam, Cambridge, MA) and 0.4 μg/ml polyclonal, C-terminal specific rabbit anti-AQP4 antibody (Santa Cruz Biotechnology). Cells were incubated for 30 min with 5 μg/ml goat anti-rabbit IgG-conjugated Alexa Fluor 555 (Invitrogen) in 1% BSA. For C9neo immunofluorescence, cells were incubated with rAbs as above, together with 2% pooled normal human complement serum. After fixation and permeabilization, cells were incubated for 60 min with 0.1 μg/ml mouse monoclonal anti-C5b-9 (C9neo) antibody and 0.4 μg/ml polyclonal, C-terminal specific rabbit anti-AQP4 antibody (both from Santa Cruz Biotechnology). Cells were then incubated for 30 min with 5 μg/ml donkey anti-mouse IgG-conjugated Alexa Fluor 488 and goat anti-rabbit IgG-conjugated Alexa Fluor 555 (Invitrogen) in 1% BSA.

Electrophoresis and Immunoblot Analysis—Cells were lysed in Blue Native buffer (500 mM ϵ-aminocaproic acid, 50 mM imidazole, pH 7.0, 12 mM NaCl, 10% glycerol, 1% Triton X-100,

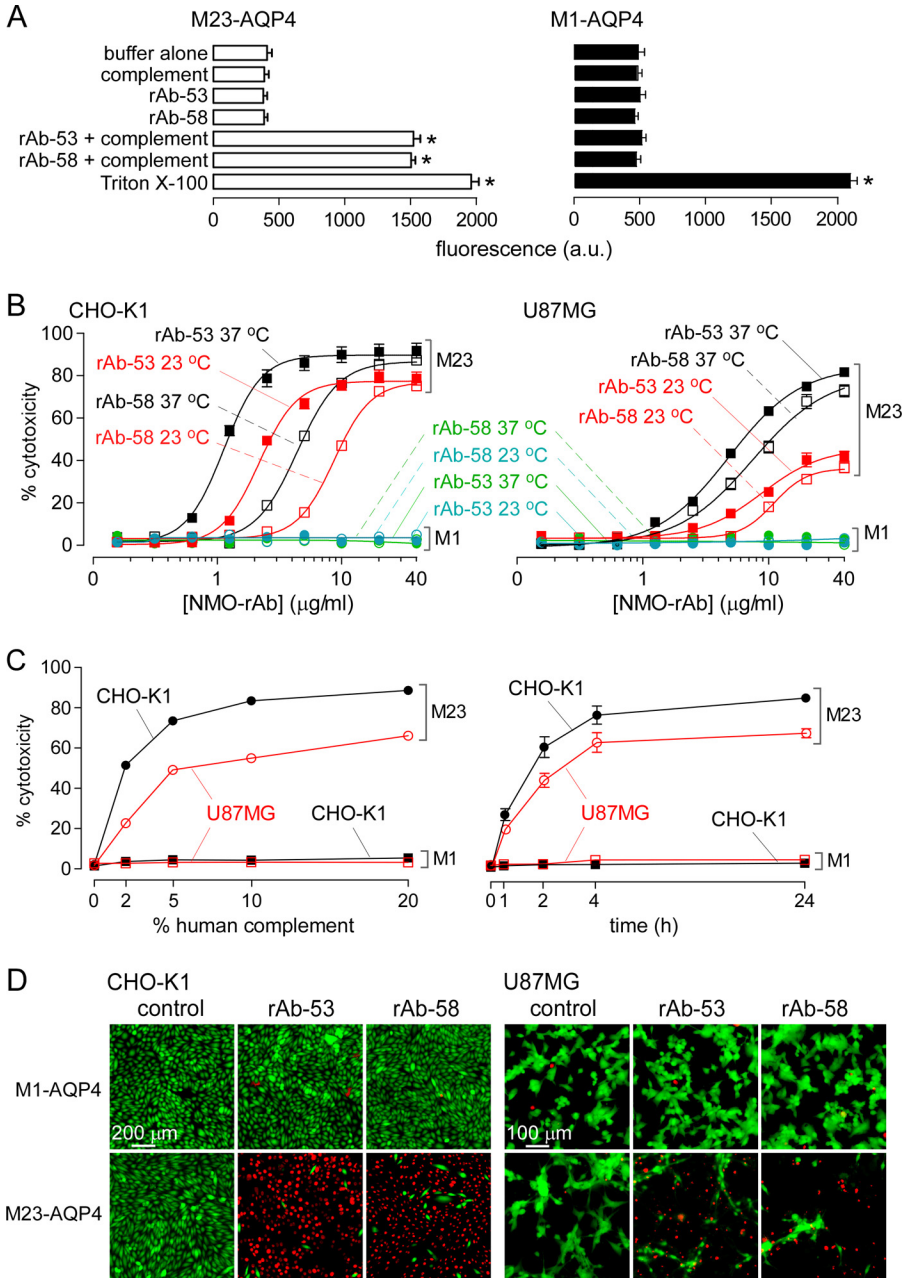

FIGURE 2. **Cells expressing M1-AQP4 are resistant to NMO-rAb/complement-mediated cytotoxicity.** *A*, LDH cytotoxicity assay showing LDH release from M1- and M23-AQP4-expressing CHO-K1 cells treated for 60 min at 37 °C with rAb-53 or rAb-58 (20 μg/ml) and/or complement (2%). Total LDH content determined by treatment with Triton X-100 (S.E., $n = 4$, *, $p < 0.01$). *B*, dependence of CDC on rAb concentration in CHO-K1 (*left*) and U87MG (*right*) cells in the presence of 2% complement (S.E., $n = 4$). Cells were incubated for 60 min with NMO-rAb and complement at 23 or 37 °C as indicated. Data were fitted to a single-site saturation model. *C*, dependence of CDC on complement concentration (*left*) and incubation time (*right*) in CHO-K1 and U87MG cells in the presence of 2.5 and 5 μg/ml rAb-58, respectively (S.E., $n = 4$). *D*, representative fluorescence micrographs showing live/dead (*green/red*) cell staining after a 60-min incubation with control or NMO rAbs and complement.

protease inhibitor mixture) and centrifuged at 22,000 × *g* for 45 min. Samples (10 μg protein) were mixed with 5% Coomassie Blue G-250 and gels were run and blotted with rabbit anti-AQP4 antibody as described (24).

RESULTS

Cells Expressing M1-AQP4 Are Resistant to CDC Caused by NMO-rAbs—Experiments were done on two different AQP4-transfected cell types to ensure robustness of the conclusions: CHO-K1 cells and U87MG cells (a human astrocyte-derived line). Fig. 1*A* shows plasma membrane targeting of the M1 and M23 isoforms of AQP4 in stably transfected CHO-K1 and U87MG cells as seen by confocal fluorescence microscopy (*top*) and TIRFM (*bottom*). AQP4 immunofluorescence was absent in nontransfected cells (not shown). M1-AQP4, which does not form OAPs, showed a smooth pattern of fluorescence, whereas M23-AQP4, which assembles in OAPs at the plasma membrane, showed a characteristic punctate pattern of fluorescence. SDS-PAGE confirmed that the transfected cells expressed exclusively M1-AQP4 or M23-AQP4 (Fig. 1*B*, *top*),

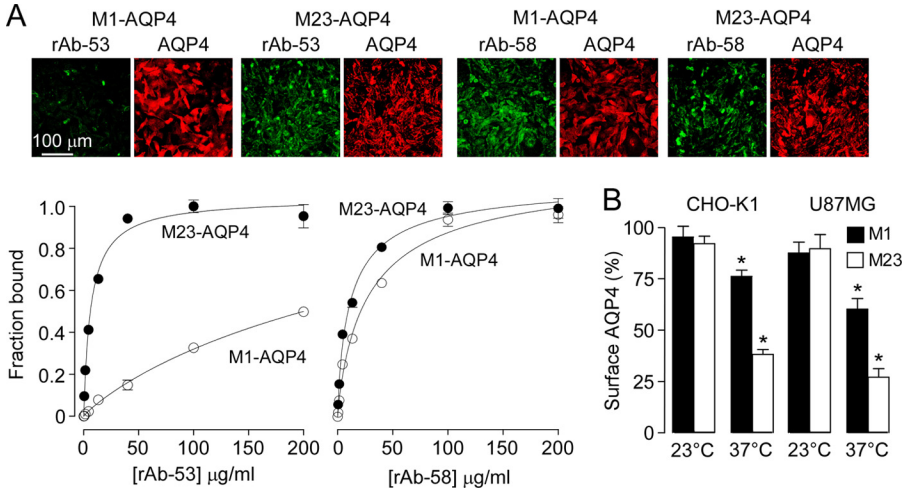

FIGURE 3. **Differences in NMO-rAb binding or AQP4 surface expression cannot account for low CDC for M1-AQP4.** *A*, *top*, representative fluorescence micrographs showing NMO-rAb (*green*) and AQP4 (*red*) immunofluorescence at 100 μg/ml rAb-53 and rAb-58 in M1- and M23-AQP4-expressing CHO cells. *Bottom*, binding curves for rAb-53 (*left*) and rAb-58 (*right*) to M1- *versus* M23-AQP4 (S.E., $n = 3$) showing green-to-red fluorescence ratios as a function of NMO-rAb concentration. Data were fitted to a single-site saturation model with fitted $K_D = 44$ nM and 2.6 μM (rAb-53) and 83 nM and 202 nM (rAb-58), for M23- and M1-AQP4, respectively. *B*, cell surface AQP4 expression at 60 min after incubation with 50 μg/ml rAb-58. Data are shown as the percentage of remaining AQP4 at the cell surface at 60 *versus* 0 min (S.E., $n = 5$, *, $p < 0.01$).

as expected. Native, nondenaturing gel electrophoresis (Blue Native-PAGE) showed a single band for M1-AQP4, indicating individual tetramers, whereas multiple high order bands were seen for M23-AQP4 because of its membrane clustering in OAPs (Fig. 1*B*, *bottom*). Fig. 1*C* shows cell surface expression of M1- and M23-AQP4. NMO antibody rAb-58, which binds to both M1-AQP4 and M23-AQP4 with similar affinity (23), was used to immunostain cell surface AQP4. The cell surface membrane marker wheat germ agglutinin was used as reference to compute the fluorescence ratio (29). There was slightly greater cell surface expression (by ~20%) of M23- as compared with M1-AQP4 in both cell lines.

An LDH fluorescence release assay was developed to quantify CDC. Fig. 2*A* shows fluorescence in the extracellular solution following cell incubation for 60 min at 37 °C with recombinant monoclonal NMO antibodies (rAb-53 or rAb-58) at 20 μg/ml and 2% human complement. Control studies (buffer alone, rAb or complement alone) showed low background signal. Incubation of M23-AQP4-expressing cells with NMO-rAbs and complement increased the LDH release fluorescence signal as compared with controls (Fig. 2*A*, *left*), whereas LDH release by M1-AQP4 cells was not increased (Fig. 2*A*, *right*), demonstrating resistance of M1-AQP4-expressing cells to CDC mediated by NMO-rAb. Antibody rAb-53 binds to M23-AQP4 with >10-fold greater affinity than to M1-AQP4, whereas rAb-58 binds to both isoforms with similar affinity (23). Fig. 2*B* summarizes cytotoxicity (percentage of LDH release referenced to 100% measured with Triton X-100) as a function of antibody concentration. LDH release was seen in cells expressing M23-AQP4 following incubation with complement and NMO antibody, but not in cells expressing M1-AQP4 at 37 and 23 °C (a temperature where AQP4 endocytosis does not occur, see below).

Cytotoxicity was measured in AQP4-expressing CHO-K1 and U87MG cells as a function of complement concentration (Fig. 2*C*, *left*) and incubation time (Fig. 2*C*, *right*). Although greater complement concentration or longer incubation time produced greater cytotoxicity in both M23-AQP4-expressing cell types, little cytotoxicity was seen in the M1-AQP4-expressing cells. Fig. 2*D* shows CDC using a different cytotoxicity assay involving live/dead cell staining. At high antibody concentration, many dead (red fluorescent) cells were seen in antibody-treated cells expressing M23-AQP4, but not in cells expressing M1-AQP4.

The resistance of M1-AQP4-expressing cells to NMO-rAb mediated CDC could be due to differences in: (*i*) NMO-rAb binding to M1- *versus* M23-AQP4; (*ii*) internalization of M1- *versus* M23-AQP4 upon NMO-rAb binding, which would protect cells against CDC; and/or (*iii*) complement activation by antibody bound to AQP4. NMO antibody binding to cell surface AQP4 under the conditions of our experiment was determined using a quantitative immunofluorescence assay in which NMO antibody is labeled green (using anti-human secondary antibody) and AQP4 is labeled red (using rabbit anti-AQP4 antibody). Fig. 3*A* shows representative fluorescence micrographs (*top*) and deduced binding curves (*bottom*) for binding of rAb-53 and rAb-58 to M1- and M23-AQP4-expressing CHO-K1 cells. NMO rAb-53 binding was greater to M23- *versus* M1-AQP4 (K_D 44 nM *versus* 2.6 μM), whereas rAb-58 binding was more similar (83 *versus* 202 nM). Importantly, under the conditions of the CDC measurements, at high antibody concentration, similar amounts of rAb-58 were bound to the M1- and M23-AQP4-expressing cells. Therefore, the resistance of M1-AQP4 to CDC cannot be explained by reduced NMO antibody binding alone.

To determine whether NMO antibody binding causes differential internalization of M1- *versus* M23-AQP4 under the condition used for CDC, we measured cell surface AQP4 after incubation with 50 μg/ml NMO rAb-58 for 1 h at both 23 °C and 37 °C, using our quantitative cell surface expression assay (29). Fig. 3*B* shows that at 37 °C, ~30 and 60% reduced cell surface AQP4 was seen for M1- and M23-AQP4 following incubation

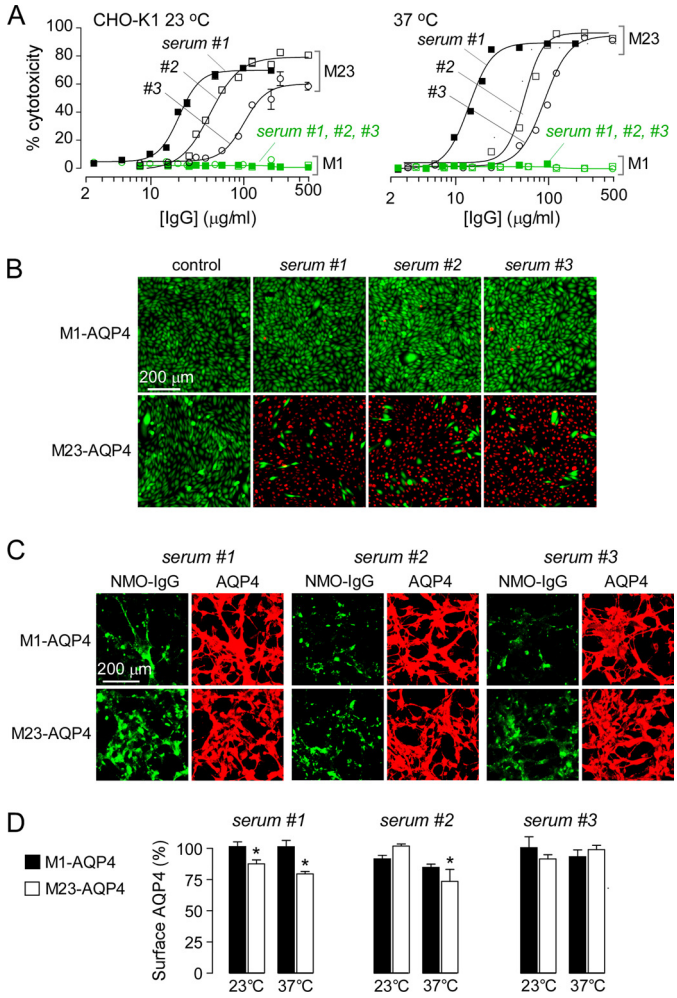

FIGURE 4. **Cells expressing M1-AQP4 are resistant to CDC caused by NMO-IgG in human NMO sera.** Total IgG was isolated from human NMO (and control) sera. *A*, dependence of cytotoxicity on total IgG concentration in the presence of 2% complement (S.E., $n = 4$). M1- and M23-AQP4-expressing CHO-K1 cells were incubated for 60 min with NMO-IgG and complement at 23 or 37 °C. *B*, representative fluorescence micrographs showing live/dead (*green/red*) cell staining after a 60-min exposure of cells to complement and control or NMO-IgGs (each 100 μg/ml). *C*, binding of NMO-IgG (each 100 μg/ml, *green*) to AQP4 (*red*) in U87MG cells expressing M1- or M23-AQP4. *D*, surface AQP4 expression in CHO-K1 cells at 60 min after incubation with 250 μg/ml NMO-IgG from NMO sera. Data are shown as the percentage of remaining AQP4 at the cell surface at 60 *versus* 0 min (S.E., $n = 5$, *, $p < 0.01$).

with rAb-58. Similar results were found in U87MG cells at 37 °C. However, cell surface AQP4 was minimally changed for both M1-AQP4 and M23-AQP4 at 23 °C in both cell lines (Fig. 3*B*). Therefore, the resistance of M1-AQP4-expressing cells to CDC is not due to reduced M1-AQP4 at the cell surface following NMO-rAb binding.

Cells Expressing M1-AQP4 Are Resistant to CDC Caused by NMO-IgG in NMO Patient Sera—Similar experiments were done with IgG isolated from NMO patient sera, which consists of a polyclonal mixture of NMO-IgGs comprising up to ~1% of total IgGs. Fig. 4*A* shows LDH release by M1- and M23-AQP4-expressing cells as a function of IgG concentration. As found for the recombinant NMO antibodies, concentration-dependent cytotoxicity was seen in cells expressing M23-AQP4 that were incubated with complement and IgG isolated from serum of three different NMO patients. Cytotoxicity was absent in cells expressing M1-AQP4. Live/dead cell staining showed independently that M1-AQP4-expressing cells were resistant to CDC (Fig. 4*B*). Cytotoxicity was absent in cells expressing M1- or M23-AQP4 with control (non-NMO) IgG. As done for the recombinant antibodies, we studied NMO antibody binding to M1- and M23-AQP4 under the conditions of CDC measurements. Fig. 4*C* shows that although serum NMO-IgG bound more tightly to M23- *versus* M1-AQP4, strong binding was found at relatively high concentrations, indicating that differences in NMO antibody binding cannot account for the near zero CDC in cells expressing M1-AQP4. We also measured cell surface AQP4 following incubation for 1 h with 250 μg/ml purified IgGs from NMO sera. Fig. 4*D* shows that cell surface M23-AQP4 was only minimally reduced under the conditions of the CDC experiments, supporting the conclusion that resistance of M1-AQP4 cells to CDC is not due to a reduced surface M1-AQP4 expression.

Resistance of M1-AQP4-expressing Cells to CDC Is Due to Absence of OAP Formation—Differences in NMO antibody-mediated CDC with M1- *versus* M23-AQP4 could be due to OAP formation by M23-AQP4 but not M1-AQP4 or to intrinsic differences in M23 *versus* M1 protein structure. To distinguish between these possibilities, CDC was measured in U87MG cells transiently expressing a point mutant of M23-AQP4 (G28P) that cannot form OAPs because of impaired N terminus intermolecular interactions (30). TIRFM (Fig. 5*A*) showed that G28P-M23-AQP4 does not form OAPs, exhibiting a smooth pattern of fluorescence similar to M1-AQP4, whereas M23-AQP4, which assembles in OAPs at the plasma membrane, showed a characteristic punctate pattern of fluorescence. Similar punctate fluorescence was also seen in U87MG cells transiently cotransfected with M23- and M1-AQP4 at ratios of 3:1 and 1:1 (Fig. 5*A*). LDH release measurements in transiently transfected cells incubated with rAb-58 and complement showed significant cytotoxicity in cells expressing M23-AQP4, but not M1-AQP4 or G28P M23-AQP4 (Fig. 5*B*). Binding measurements showed that the absence of cytotoxicity in cells expressing G28P-M23 was not due to greatly reduced NMO antibody binding (Fig. 5*C*). CDC was also measured in cells transiently transfected with M1- and M23-AQP4 in different ratios. We previously showed that the resultant cells coexpress M1- and M23-AQP4 protein in approximately the same ratios as those of the plasmids used for transfection (23). Although cotransfection of M23 and M1 at a ratio of 3:1 had little effect on cytotoxicity as compared with cells expressing M23 alone, cytotoxicity was reduced at an M23 to M1 ratio 1:1 (Fig. 5*B*), with little effect on NMO antibody binding (Fig. 5*C*). Analysis of immunostaining data showed similar cell surface expression of M1-, M23-, and G28P-M23-AQP4 in the transiently transfected U87MG cells, as well as AQP4 at the different M1:M23 ratios. Together, these studies support the conclusion that AQP4 assembly in OAPs is required for CDC.

ADCC Is Not Dependent on OAP Formation by AQP4—Although CDC is probably the principal mechanism of cytotoxicity in NMO, there is evidence as well for ADCC involving NK cells and perhaps granulocytes as effector cells (9). We investigated whether OAP assembly by AQP4 is required for ADCC. AQP4-expressing cells were incubated with NMO antibody

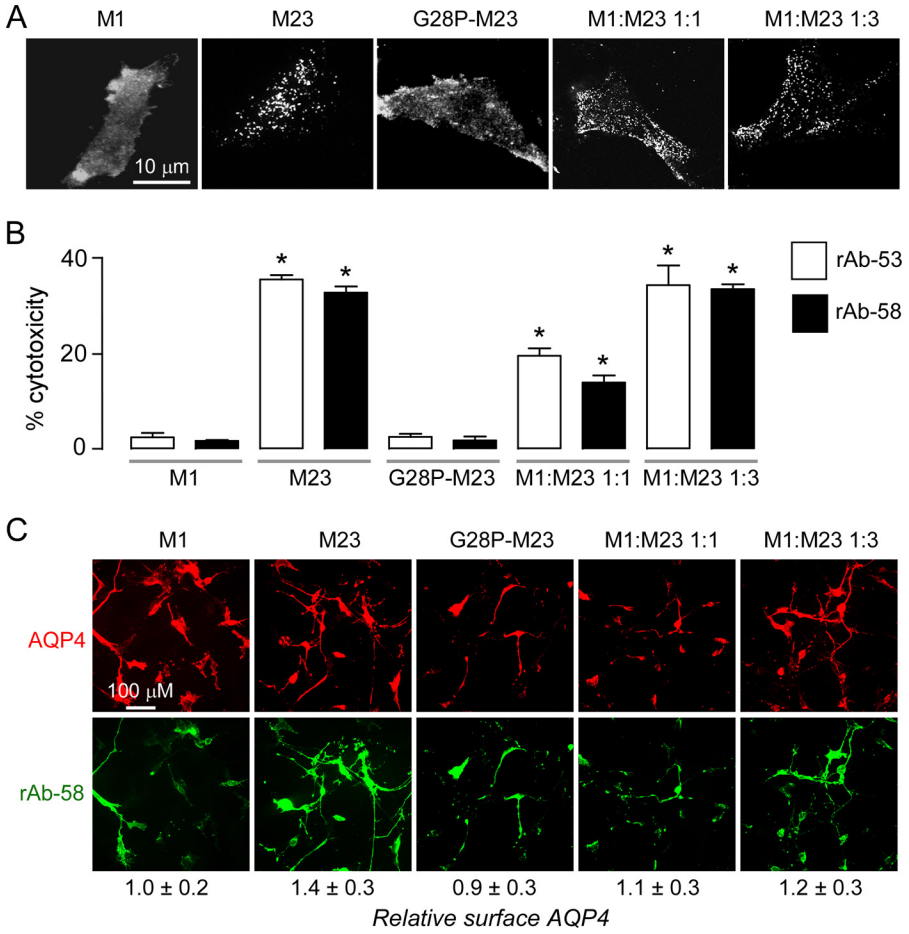

FIGURE 5. **AQP4 assembly in OAPs is required for CDC.** U87MG cells were transiently transfected with M1- or M23-AQP4, G28P-M23-AQP4 (OAP-disrupting mutation), or the indicated mixtures of M1- and M23-AQP4. *A*, TIRFM of transfected cells immunostained with anti-AQP4 antibody. *B*, CDC assay on transfected cells (S.E., $n = 4$, *, $p < 0.001$). *C*, fluorescence micrographs of transfected cells stained with 20 μg/ml rAb-58 (*green*) and anti-AQP4 antibody (*red*). Values for relative AQP4 cell surface expression are shown, normalized to that of M1-AQP4 (S.E., $n = 3$).

and human NK cells. Cytotoxicity was assayed by live/dead cell staining (as LDH measurements are confounded by LDH released from effector cells). In contrast to the results for CDC, efficient ADCC was found in cells expressing M1- or M23-AQP4 (Fig. 6*A*). At high antibody concentration (100 μg/ml), where NMO rAb-58 binding is comparable in cells expressing M1- and M23-AQP4, ADCC was comparable. ADCC was more efficient in M23- than in M1-AQP4-expressing cells when incubated with rAb-53, as expected from its differential binding (as was shown in Fig. 3*A*). Our results indicate that in contrast to CDC, ADCC was observed in both M1-AQP4-expressing and M23-AQP4-expressing cells, whose efficiency was determined by NMO antibody binding but not by AQP4 OAP formation.

AQP4 OAPs Increase C1q Binding and Complement Activation by AQP4-bound NMO-IgG—We postulated that AQP4 OAPs are required for CDC but not ADCC because CDC involves multivalent binding of complement protein C1q to clustered NMO-IgG on OAPs, whereas ADCC involves monovalent interaction of NMO-IgG to Fc receptors on effector cells. C1q binding to AQP4-bound rAb-58 was measured using an anti-C1q antibody following incubation of AQP4-expressing cells with NMO antibody and purified C1q protein. Fig. 7*A* (*left*) shows comparable binding of 40 μg/ml rAb-58 to M1- and

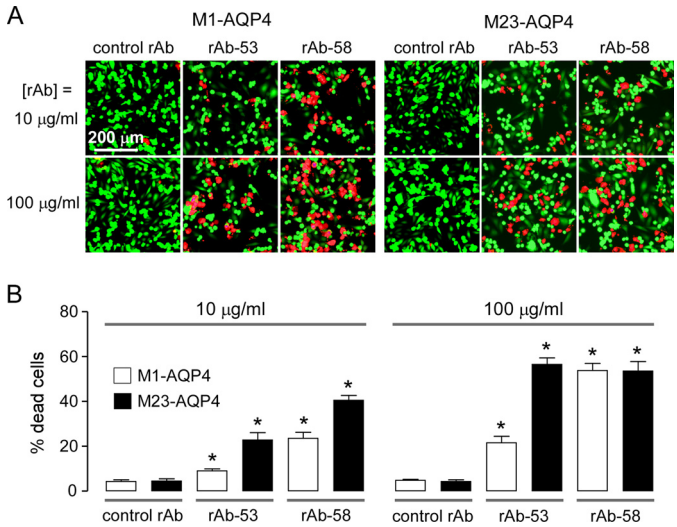

FIGURE 6. **ADCC does not depend on AQP4 OAP formation.** *A*, live/dead (*red*/*green*) staining of M1- and M23-AQP4-expressing CHO-K1 cells incubated with NK cells and 10 or 100 μg/ml control rAb, rAb-53, or rAb-58. *B*, the percentage of dead cells (*red*/(*red* + *green*)) (S.E., $n = 4–6$, *, $p < 0.01$).

M23-AQP4-expressing cells. Fig. 7*A* (*center panels*) shows substantially greater C1q binding to cells expressing M23 *versus* M1-AQP4 when rAb-58 was present. Fig. 7*A* (*right*) shows sim-

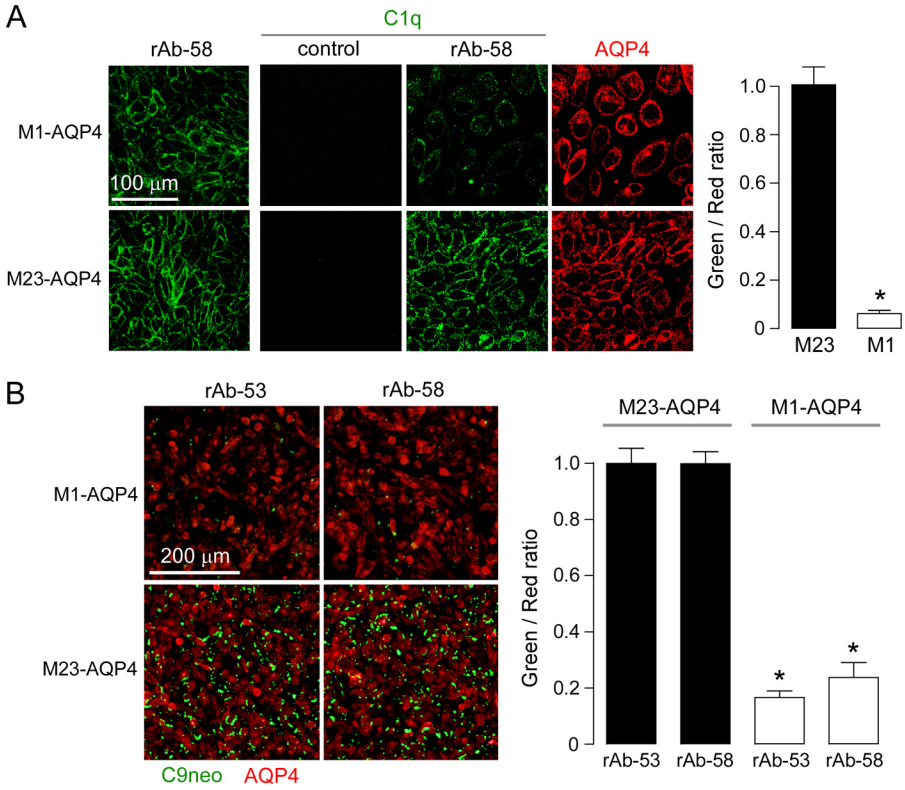

FIGURE 7. **Greatly reduced C1q binding to NMO-IgG accounts for resistance of M1-AQP4-expressing cells to CDC.** *A*, *left*, staining of M1- and M23-AQP4 in CHO-K1 cells with 40 μg/ml NMO rAb-58. *Center panels*, C1q staining. Cells were incubated with 40 μg/ml rAb-58 (or control rAb) and 120 μg/ml purified recombinant C1q for 30 min, fixed, and stained with FITC-conjugated anti-C1q antibody. AQP4 was stained red with anti-AQP4 antibody. *Right*, green-to-red fluorescence ratio (S.E., $n = 4$, *, $p < 0.001$). *B*, C9neo immunostaining. *Left*, cells were incubated with 20 μg/ml rAb-53 or rAb-58 and 2% complement for 30 min, fixed, and stained with anti-C9neo antibody and green fluorescent secondary antibody. AQP4 was stained red. *Right*, green-to-red fluorescence ratio (S.E., $n = 4$, *, $p < 0.001$).

ilar AQP4 expression. Data were quantified as green-to-red fluorescence ratios (Fig. 7*A*, *right*). Reduced C1q binding is predicted to translate to reduced formation of the complement attack complex and consequent cytotoxicity. Fig. 7*B* confirms greatly reduced complement attack complex on M1-AQP4-expressing cells following incubation with NMO-rAbs and complement, as revealed by C9neo antibody immunofluorescence.

DISCUSSION

Complement-dependent cytotoxicity in NMO depends on the level of AQP4 expression at the cell surface and its supramolecular assembly state, NMO antibody binding, and potentially other factors such as complement regulator proteins. We reported previously that the affinity of NMO antibody binding to AQP4 is generally much greater when AQP4 is assembled in OAPs than as separate tetramers, sometimes by a factor of 10 or greater, although some antibodies recognize OAP-assembled and tetrameric AQP4 with comparable affinity (23). We discovered here a second mechanism, independent of NMO antibody binding, by which AQP4 assembly in OAPs greatly increases CDC. As such, maneuvers that interfere with AQP4 association in OAPs may greatly reduce CDC in NMO by acting on two separate steps, producing multiplicative effects.

Our results support the conclusion that the greatly enhanced CDC for OAP-assembled AQP4 is the consequence of the multivalent interaction of complement protein C1q with array-assembled NMO-IgG. Complement protein C1 is composed of three glycoproteins, C1q, C1r, and C1s. C1q contains six globular heads, each having a binding site for the Fc region of IgG and connected to a central subunit by a collagen-like strand (31–33). C1r and C1s, which bind at the connecting region of C1q, are proenzymes that are converted to active proteases upon binding to C1q (26). Complement activation requires at least bivalent binding of C1q to IgG (34). The low binding affinity of C1q to an IgG monomer ($1–5 \times 10^4$ M^{-1}) allows rapid dissociation of the C1q-IgG complex, preventing conversion of C1r-C1s into active proteases (25, 35). The binding affinity of C1q to IgG increases by at least 1000-fold (5×10^7 M^{-1} for bivalent binding, 10^{10} M^{-1} for trivalent binding) (36) when C1q binds to two (or more) adjacent IgG molecules. Formation of relatively stable multivalent C1q-IgG complexes allows for efficient activation of C1r-C1s to initiate complement activation. As diagrammed in Fig. 8, the size and geometry of AQP4 OAPs, bound NMO-IgG, and C1q allow for multivalent C1q interaction with NMO-IgG when clustered on AQP4 OAPs. Multivalent C1q binding to NMO-IgG on separate AQP4 tetramers, which would require at least dimerization of separate, mobile AQP4 tetramers, is an inefficient process. We note that the complement pathway can also be activated by mannose-binding protein binding to a specific glycoform of IgG (33). Mannose-binding protein has a tetravalent structure with similar geometry to that of C1q, also allowing multivalent interaction with OAP-assembled NMO-IgG.

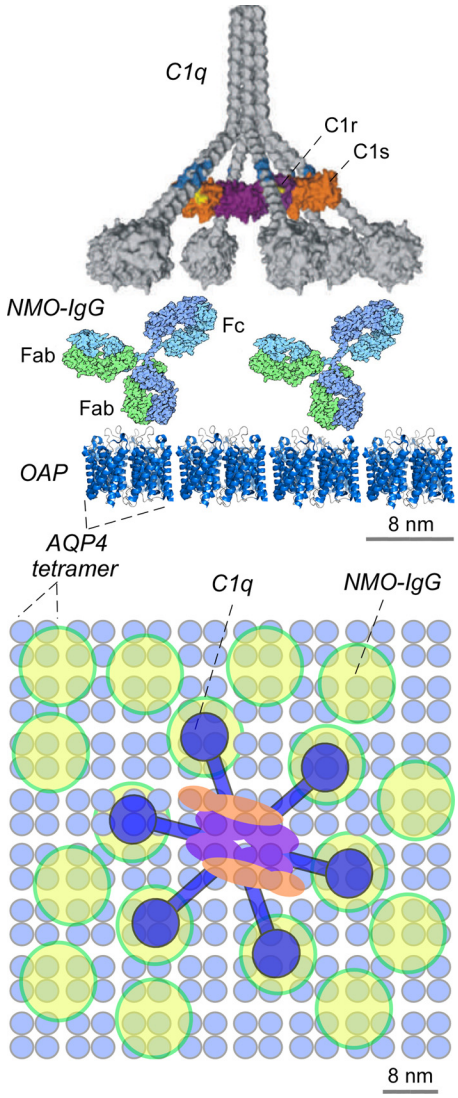

FIGURE 8. **Schematic showing multivalent binding of C1q to Fc regions of NMO-IgG bound to OAP-assembled AQP4.** Side view (*top*) and en-face view (*bottom*) are shown. Proteins in each view shown on the same size scales as indicated.

In contrast to CDC, interaction of effector cells with NMO antibody in ADCC does not involve multivalent interaction (38) and so does not require AQP4 clustering in OAPs. It is generally believed that CDC is more important than ADCC in NMO disease pathogenesis (1, 39, 40); however, direct evidence remains lacking. Involvement of ADCC in NMO would have important implications for NMO therapeutics targeting AQP4 supramolecular assembly.

Several prior studies have reported CDC in primary astrocytes and various AQP4-transfected cell lines using human NMO sera, although the significance of OAP-dependent CDC was not appreciated because of differences in the expressed constructs, cell types, NMO sera, complement incubation conditions, and cytotoxicity read-outs. CDC was demonstrated using a tetrazolium-based viability assay in primary astrocyte cultures, which expresses both M1-AQP4 and M23-AQP4 when exposed to a 1:50 dilution of NMO serum and 1% complement (41). Propidium iodide viability assays showed CDC in HEK293 cells transfected with a green fluorescent protein-M1-AQP4 chimera and exposed to a 1:5 dilution of NMO serum and 20% active complement (42). CDC was also observed by flow cytometry following a 12-h incubation of M1-AQP4-transfected LN18 astrocytoma cells with NMO-IgG and complement (9). Although these studies showed NMO-IgG-dependent CDC in AQP4-expressing primary and transfected cells, they did not consider AQP4 isoform effects or OAPs. During the preparation of our manuscript, Hinson *et al.* (43) reported reduced CDC in HEK293 cells transfected with M1- *versus* M23-AQP4 following incubation with NMO patient serum and complement. They speculated that the difference was due to reduced cell surface expression of M1-AQP4 because of internalization. Our data show that the difference in CDC efficiency is not due to AQP4 internalization or differences in NMO-IgG binding affinity, but is instead the consequence of enhanced C1q binding to clustered NMO-IgG on AQP4 OAPs.

The assembly of M23-AQP4 in OAPs involves intermolecular N terminus interactions of residues just downstream of M23 (30). M1-AQP4 does not form OAPs by itself because of disruption of these N terminus interactions by residues upstream of M23. M1- and M23-AQP4 comingle in heterotetramers when coexpressed (44, 45), producing smaller OAPs with increasing ratio of M1:M23-AQP4 protein (28, 46). Mathematical modeling provided a quantitative explanation of M1:M23 ratio-dependent OAP size, in which M1-AQP4 monomers localize to the periphery of OAPs, preventing their growth (47). The modeling also made the experimentally verified prediction that OAP shape depends on M1:M23 ratio, with relative elongation of intermediate-size OAPs. Based on modeling considerations, we predict reduced CDC for an elongated *versus* square OAP of the same area. With regard to CDC and NMO disease pathogenesis, AQP4 OAPs in astrocytes coexpress M1-AQP4 and M23-AQP4 and are of intermediate size, such that relatively minor changes in M1:M23 ratio may considerably alter CDC efficiency. In addition, AQP4 OAPs are dynamic structures in which altered M1-AQP4 palmitoylation can reduce OAP size, as can various intracellular signaling events involving protein kinases and calcium signaling (44, 48). A consequence of the dual effect of OAP assembly on NMO antibody binding and CDC is the potential utility of targeting OAP formation by AQP4 for NMO therapy. OAP-targeted therapies might include small-molecule disrupters of OAP assembly, transcriptional regulators that increase M1-AQP4 expression, or effectors of palmitoylation or other signaling processes. An OAP-targeted therapy is predicted to reduce NMO pathology by itself or in conjunction with conventional therapies such as immunosuppression or plasmapheresis, or therapies under development such as monoclonal antibody blockers of NMO-IgG binding to AQP4.

The targeting of pathogenic autoantibodies to a stably aggregated target makes NMO a unique CDC-dependent autoimmune disease. There are autoimmune diseases associated with excessive complement activation (49), including paroxysmal nocturnal hemoglobinuria, in which erythrocyte resistance to complement is reduced because of defective complement regulator protein function (50), and a subgroup of atypical hemolytic-uremic syndrome caused by deficiency of complement regulatory protein factor H (51, 52). More closely related com-

plement-dependent autoimmune diseases include myasthenia gravis, where autoantibodies targeting the nicotinic acetylcholine receptor cause complement activation, decreased receptor expression, and muscle weakness (53), and anti-neutrophil cytoplasmic antibody-associated vasculitis, producing Churg-Strauss syndrome, microscopic polyangiitis, and Wegener granulomatosis (37). The targeting of NMO-IgG to stable aggregates of surface-exposed AQP4 makes NMO a unique autoimmune disease in which AQP4 OAP assembly confers strong sensitivity to complement.

In conclusion, our results establish a second mechanism by which AQP4 assembly in OAPs regulates NMO-IgG-dependent CDC in NMO. Our data suggest OAP disruption as a therapeutic approach in NMO to reduce astrocyte cytotoxicity without altering AQP4-dependent water permeability and hence astrocyte function.

Acknowledgments—We thank Dr. Jeffrey Bennett (University of Colorado, Aurora, CO) for providing monoclonal recombinant antibodies and Joseph Tan for technical assistance with binding studies.

REFERENCES

1. Wingerchuk, D. M., Lennon, V. A., Lucchinetti, C. F., Pittock, S. J., and Weinshenker, B. G. (2007) The spectrum of neuromyelitis optica. *Lancet Neurol.* **6,** 805–815
2. Jarius, S., Paul, F., Franciotta, D., Waters, P., Zipp, F., Hohlfeld, R., Vincent, A., and Wildemann, B. (2008) Mechanisms of disease: aquaporin-4 antibodies in neuromyelitis optica. *Nat. Clin. Pract. Neurol.* **4,** 202–214
3. Lucchinetti, C. F., Mandler, R. N., McGavern, D., Bruck, W., Gleich, G., Ransohoff, R. M., Trebst, C., Weinshenker, B., Wingerchuk, D., Parisi, J. E., and Lassmann, H. (2002) A role for humoral mechanisms in the pathogenesis of Devic's neuromyelitis optica. *Brain* **125,** 1450–1461
4. Misu, T., Fujihara, K., Kakita, A., Konno, H., Nakamura, M., Watanabe, S., Takahashi, T., Nakashima, I., Takahashi, H., and Itoyama, Y. (2007) Loss of aquaporin-4 in lesions of neuromyelitis optica: distinction from multiple sclerosis. *Brain* **130,** 1224–1234
5. Lennon, V. A., Wingerchuk, D. M., Kryzer, T. J., Pittock, S. J., Lucchinetti, C. F., Fujihara, K., Nakashima, I., and Weinshenker, B. G. (2004) A serum autoantibody marker of neuromyelitis optica: distinction from multiple sclerosis. *Lancet* **364,** 2106–2112
6. Lennon, V. A., Kryzer, T. J., Pittock, S. J., Verkman, A. S., and Hinson, S. R. (2005) IgG marker of optic-spinal multiple sclerosis binds to the aquaporin-4 water channel. *J. Exp. Med.* **202,** 473–477
7. Nielsen, S., Nagelhus, E. A., Amiry-Moghaddam, M., Bourque, C., Agre, P., and Ottersen, O. P. (1997) Specialized membrane domains for water transport in glial cells: high-resolution immunogold cytochemistry of aquaporin-4 in rat brain. *J. Neurosci.* **17,** 171–180
8. Rash, J. E., Yasumura, T., Hudson, C. S., Agre, P., and Nielsen, S. (1998) Direct immunogold labeling of aquaporin-4 in square arrays of astrocyte and ependymocyte plasma membranes in rat brain and spinal cord. *Proc. Natl. Acad. Sci. U.S.A.* **95,** 11981–11986
9. Bennett, J. L., Lam, C., Kalluri, S. R., Saikali, P., Bautista, K., Dupree, C., Glogowska, M., Case, D., Antel, J. P., Owens, G. P., Gilden, D., Nessler, S., Stadelmann, C., and Hemmer, B. (2009) Intrathecal pathogenic anti-aquaporin-4 antibodies in early neuromyelitis optica. *Ann. Neurol.* **66,** 617–629
10. Bradl, M., Misu, T., Takahashi, T., Watanabe, M., Mader, S., Reindl, M., Adzemovic, M., Bauer, J., Berger, T., Fujihara, K., Itoyama, Y., and Lassmann, H. (2009) Neuromyelitis optica: pathogenicity of patient immunoglobulin *in vivo*. *Ann. Neurol.* **66,** 630–643
11. Kinoshita, M., Nakatsuji, Y., Kimura, T., Moriya, M., Takata, K., Okuno, T., Kumanogoh, A., Kajiyama, K., Yoshikawa, H., and Sakoda, S. (2009) Neuromyelitis optica: passive transfer to rats by human immunoglobulin. *Biochem. Biophys. Res. Commun.* **386,** 623–627
12. Saadoun, S., Waters, P., Bell, B. A., Vincent, A., Verkman, A. S., and Papadopoulos, M. C. (2010) Intra-cerebral injection of neuromyelitis optica immunoglobulin G and human complement produces neuromyelitis optica lesions in mice. *Brain* **133,** 349–361
13. Roemer, S. F., Parisi, J. E., Lennon, V.A., Benarroch, E. E., Lassmann, H., Bruck, W., Mandler, R. N., Weinshenker, B. G., Pittock, S. J., Wingerchuk, D. M., and Lucchinetti, C. F. (2007) Pattern-specific loss of aquaporin-4 immunoreactivity distinguishes neuromyelitis optica from multiple sclerosis. *Brain* **130,** 1194–1205
14. Hinson, S. R., Pittock, S. J., Lucchinetti, C. F., Roemer, S. F., Fryer, J. P., Kryzer, T. J., and Lennon, V. A. (2007) Pathogenic potential of IgG binding to water channel extracellular domain in neuromyelitis optica. *Neurology* **69,** 2221–2231
15. Cree, B. A., Lamb, S., Morgan, K., Chen, A., Waubant, E., and Genain, C. (2005) An open label study of the effects of rituximab in neuromyelitis optica. *Neurology* **64,** 1270–1272
16. Miyamoto, K., and Kusunoki, S. (2009) Intermittent plasmapheresis prevents recurrence in neuromyelitis optica. *Ther. Apher. Dial.* **13,** 505–508
17. Tradtrantip, L., Zhang, H., Saadoun, S., Phuan, P., Lam, C., Papdopoulos, M. C., Bennett, J. L., and Verkman, A. S. (2012) Anti–Aquaporin-4 monoclonal antibody blocker therapy for neuromyelitis optica. *Ann. Neurol.* **71,** 314–322
18. Landis, D. M., and Reese, T. S. (1974) Arrays of particles in freeze-fractured astrocytic membranes. *J. Cell Biol.* **60,** 316–320
19. Wolburg, H. (1995) Orthogonal arrays of intramembranous particles: a review with special reference to astrocytes. *J. Hirnforsch.* **36,** 239–258
20. Hasegawa, H., Ma, T., Skach, W., Matthay, M. A., and Verkman, A. S. (1994) Molecular cloning of a mercurial-insensitive water channel expressed in selected water-transporting tissues. *J. Biol. Chem.* **269,** 5497–5500
21. Yang, B., Brown, D., and Verkman, A. S. (1996) The mercurial insensitive water channel (AQP-4) forms orthogonal arrays in stably transfected Chinese hamster ovary cells. *J. Biol. Chem.* **271,** 4577–4580
22. Verbavatz, J. M., Ma, T., Gobin, R., and Verkman, A. S. (1997) Absence of orthogonal arrays in kidney, brain, and muscle from transgenic knockout mice lacking water channel aquaporin-4. *J. Cell Sci.* **110,** 2855–2860
23. Crane, J. M., Lam, C., Rossi, A., Gupta, T., Bennett, J. L., and Verkman, A. S. (2011) Binding affinity and specificity of neuromyelitis optica autoantibodies to aquaporin-4 M1/M23 isoforms and orthogonal arrays. *J. Biol. Chem.* **286,** 16516–16524
24. Rossi, A., Baumgart, F., van Hoek, A. N., and Verkman, A. S. (2012) Post-Golgi supramolecular assembly of aquaporin-4 in orthogonal arrays. *Traffic* **13,** 43–53
25. Sledge, C. R., and Bing, D. H. (1973) Binding properties of the human complement protein C1q. *J. Biol. Chem.* **248,** 2818–2823
26. Duncan, A. R., and Winter, G. (1988) The binding site for C1q on IgG. *Nature* **332,** 738–740
27. Eggleton, P., Reid, K. B., and Tenner, A. J. (1998) C1q: How many functions? How many receptors? *Trends Cell Biol.* **8,** 428–431
28. Crane, J. M., Rossi, A., Gupta, T., Bennett, J. L., and Verkman, A. S. (2011) Orthogonal array formation by human aquaporin-4: examination of neuromyelitis optica-associated aquaporin-4 polymorphisms. *J. Neuroimmunol.* **236,** 93–98
29. Ratelade, J., Bennett, J. L., and Verkman, A. S. (2011) Evidence against cellular internalization *in vivo* of NMO-IgG, aquaporin-4, and excitatory amino acid transporter 2 in neuromyelitis optica. *J. Biol. Chem.* **286,** 45156–45164
30. Crane, J. M., and Verkman, A. S. (2009) Determinants of aquaporin-4 assembly in orthogonal arrays revealed by live-cell single-molecule fluorescence imaging. *J. Cell Sci.* **122,** 813–821
31. Reid, K. B. (1983) Proteins involved in the activation and control of the two pathways of human complement. *Biochem. Soc. Trans.* **11,** 1–12
32. Sellar, G. C., Blake, D. J., and Reid, K. B. (1991) Characterization and organization of the genes encoding the A-, B- and C-chains of human complement subcomponent C1q: the complete derived amino acid sequence of human C1q. *Biochem. J.* **274,** 481–490
33. Wallis, R., Mitchell, D. A., Schmid, R., Schwaeble, W. J., and Keeble, A. H.

(2010) Paths reunited: initiation of the classical and lectin pathways of complement activation. *Immunobiology* **215,** 1–11
34. Schumaker, V. N., Hanson, D. C., Kilchherr, E., Phillips, M. L., and Poon, P. H. (1986) A molecular mechanism for the activation of the first component of complement by immune complexes. *Mol. Immunol.* **23,** 557–565
35. Schumaker, V. N., Calcott, M. A., Spiegelberg, H. L., and Müller-Eberhard, H. J. (1976) Ultracentifuge studies of the binding of IgG of different subclasses to the C1q subunit of the first component of complement. *Biochemistry* **15,** 5175–5181
36. Hughes-Jones, N. C. (1977) Functional affinity constants of the reaction between ^{125}I-labeled C1q and C1q binders and their use in the measurement of plasma C1q concentrations. *Immunology* **32,** 191–198
37. Wilde, B., van Paassen, P., Witzke, O., and Tervaert, J. W. (2011) New pathophysiological insights and treatment of ANCA-associated vasculitis. *Kidney Int.* **79,** 599–612
38. Gessner, J. E., Heiken, H., Tamm, A., and Schmidt, R. E. (1998) The IgG Fc receptor family. *Ann. Hematol.* **76,** 231–248
39. Kalluri, S. R., Illes, Z., Srivastava, R., Cree, B., Menge, T., Bennett, J. L., Berthele, A., and Hemmer, B. (2010) Quantification and functional characterization of antibodies to native aquaporin-4 in neuromyelitis optica. *Arch. Neurol.* **67,** 1201–1208
40. Jarius, S., and Wildemann, B. (2010) AQP4 antibodies in neuromyelitis optica: diagnostic and pathogenetic relevance. *Nat. Rev. Neurol.* **6,** 383–392
41. Sabater, L., Giralt, A., Boronat, A., Hankiewicz, K., Blanco, Y., Llufriu, S., Alberch, J., Graus, F., and Saiz, A. (2009) Cytotoxic effect of neuromyelitis optica antibody (NMO-IgG) to astrocytes: an *in vitro* study. *J. Neuroimmunol.* **215,** 31–35
42. Hinson, S. R., McKeon, A., Fryer, J. P., Apiwattanakul, M., Lennon, V. A., and Pittock, S. J. (2009) Prediction of neuromyelitis optica attack severity by quantitation of complement-mediated injury to aquaporin-4-expressing cells. *Arch. Neurol.* **66,** 1164–1167
43. Hinson, S. R., Romero, M. F., Popescu, B. F., Lucchinetti, C. F., Fryer, J. P., Wolburg, H., Fallier-Becker, P., Noell, S., and Lennon, V. A. (2012) Molecular outcomes of neuromyelitis optica (NMO)-IgG binding to aquaporin-4 in astrocytes. *Proc. Natl. Acad. Sci. U.S.A.* **109,** 1245–1250
44. Crane, J. M., Bennett, J. L., and Verkman, A. S. (2009) Live cell analysis of aquaporin-4 M1/M23 interactions and regulated orthogonal array assembly in glial cells. *J. Biol. Chem.* **284,** 35850–35860
45. Tajima, M., Crane, J. M., and Verkman, A. S. (2010) Aquaporin-4 (AQP4) associations and array dynamics probed by photobleaching and single-molecule analysis of green fluorescent protein-AQP4 chimeras. *J. Biol. Chem.* **285,** 8163–8170
46. Furman, C. S., Gorelick-Feldman, D. A., Davidson, K. G., Yasumura, T., Neely, J. D., Agre, P., and Rash, J. E. (2003) Aquaporin-4 square array assembly: opposing actions of M1 and M23 isoforms. *Proc. Natl. Acad. Sci. U.S.A.* **100,** 13609–13614
47. Jin, B. J., Rossi, A., and Verkman, A. S. (2011) Model of aquaporin-4 supramolecular assembly in orthogonal arrays based on heterotetrameric association of M1-M23 isoforms. *Biophys. J.* **100,** 2936–2945
48. Crane, J. M., Van Hoek, A. N., Skach, W. R., and Verkman, A. S. (2008) Aquaporin-4 dynamics in orthogonal arrays in live cells visualized by quantum dot single particle tracking. *Mol. Biol. Cell* **19,** 3369–3378
49. Daha, N. A., Banda, N. K., Roos, A., Beurskens, F. J., Bakker, J. M., Daha, M. R., and Trouw, L. A. (2011) Complement activation by (auto-) antibodies. *Mol. Immunol.* **48,** 1656–1665
50. Parker, C., Omine, M., Richards, S., Nishimura, J., Bessler, M., Ware, R., Hillmen, P., Luzzatto, L., Young, N., Kinoshita, T., Rosse, W., and Socié, G. (2005) Diagnosis and management of paroxysmal nocturnal hemoglobinuria. *Blood* **106,** 3699–3709
51. Skerka, C., Zipfel, P. F., Müller, D., Micklisch, S., Riedl, M., Zimmerhackl, L. B., and Hofer, J. (2010) The autoimmune disease DEAP-hemolytic uremic syndrome. *Semin. Thromb. Hemost.* **36,** 625–632
52. Loirat, C., and Frémeaux-Bacchi, V. (2011) Atypical hemolytic uremic syndrome. *Orphanet J. Rare Dis.* **6,** 60–90
53. Gomez, A. M., Van Den Broeck, J., Vrolix, K., Janssen, S. P., Lemmens, M. A., Van Der Esch, E., Duimel, H., Frederik, P., Molenaar, P. C., Martínez-Martínez, P., De Baets, M. H., and Losen, M. (2010) Antibody effector mechanisms in myasthenia gravis pathogenesis at the neuromuscular junction. *Autoimmunity* **43,** 353–370